

# Attractor-Keyed Memory

Natalia G. Berloff<sup>1</sup>

<sup>1</sup>*Department of Applied Mathematics and Theoretical Physics,  
University of Cambridge, Cambridge CB3 0WA, United Kingdom\**

Physical selectors (lasers choosing a mode, Ising machines settling on a ground state, condensates occupying a spin state) produce high-dimensional signatures at the moment of decision: full field amplitudes, multimode interference patterns, or scattering responses. These signatures are richer than the winner’s index, yet they are routinely discarded. We show that when the signatures are repeatable across trials (stereotyped) and linearly independent across routes, a single linear decoder compiled from calibration data maps them to arbitrary payloads, merging selection and memory access into one event and eliminating the fetch that dominates latency and energy in sparse routing architectures. The construction requires one SVD of measured device responses, which certifies capability and bounds worst-case error for any downstream payload before the task is chosen. Runtime error separates into two independently diagnosable channels, decoding fidelity (controlled by dictionary conditioning  $\sigma_{\min}(\Phi)$ ) and routing reliability (controlled by the margin-to-noise ratio  $\Delta/T_{\text{eff}}$ ), each with a distinct physical origin and targeted remedy. We derive the full error decomposition, give Ising-machine selector constructions, and validate the predicted scalings on synthetic speckle-signature simulations across three measurement modalities. No hardware demonstration exists; we provide a falsifiable four-step experimental protocol specifying what a first experiment must measure. Whether real device signatures satisfy stereotypy is the central open question.

Architectures built around discrete selection, including mixture-of-experts models [1], neuromorphic processors [2, 3], and photonic classifiers [4, 5], perform two operations per input: a router selects which of  $K$  experts (or lookup-table rows) to activate, then the associated  $D$ -dimensional payload is fetched from digital memory [6–9]. The fetch is the bottleneck: in large sparse models the payload read dominates both latency and energy [2, 7]. Yet the physics of selection has already produced a rich observable at the moment of decision.

When a laser selects a mode, a condensate occupies a state [10], or an Ising machine relaxes toward a ground-state configuration [11–13], the winning attractor carries a high-dimensional physical signature (a full field amplitude, a multimode interference pattern, or a scattering response) far richer than the winner’s index. This signature is discarded. We show that a fixed linear decoder can map it to arbitrary associated data, so that selection and memory access become a single event. We call this primitive *attractor-keyed memory* (AKM); retrieval without a separate memory fetch we term *fetchless lookup*.

The framework rests on one physical assumption and one algebraic condition. The assumption is *route-conditioned repeatability* (stereotypy): conditioned on route  $k$  winning, the measured signature is approximately the same regardless of which input triggered the selection. Given stereotypy, the algebraic condition is that the  $K$  calibrated mean signatures must be linearly independent. When they are, a minimum-norm pseudoinverse decoder [14]  $W = Y\Phi^+$  recovers any desired payload table  $Y$  exactly, where  $\Phi \in \mathbb{R}^{M_{\text{sig}} \times K}$  collects the  $K$  mean signatures of dimension  $M_{\text{sig}}$ . Since  $\Phi$  depends only on the hardware, changing the payload requires only recompiling  $W$ , not modifying the selector or recalibrating.

AKM reframes the design target for physical comput-

ing hardware: instead of optimizing only for fast winner selection, *engineer the post-selection state so its signatures form a well-conditioned dictionary*. This reframing yields three practical consequences. First, a *task-independent certification protocol*: a single SVD of measured device responses determines  $\text{rank}(\Phi)$  and  $\sigma_{\min}(\Phi)$ , certifying whether universal payload realizability holds and bounding worst-case error for *any* downstream payload before deployment. Second, a two-channel error decomposition with distinct diagnostics and remedies: decoding fidelity controlled by  $\sigma_{\min}(\Phi)$ , routing reliability controlled by the ratio  $\Delta/T_{\text{eff}}$  of the selection margin to effective noise temperature. Third, concrete hardware design targets: three predeployment failure modes (rank loss, conditioning collapse, margin collapse) that are each measurable and separately remediable.

The underlying linear algebra (pseudoinverse solvability, singular-value conditioning) is standard [14]; the rank criterion for  $\Phi$  is the finite-dictionary analogue of the full-rank condition in reservoir readout training [15, 16]. In reservoir computing [16, 17], readout noise and selection errors fold into a single error budget discovered empirically per task; in Hopfield retrieval [18], the attractor *is* the stored object and there is no separate decoding channel. The novelty is the object the algebra acts on:  $\Phi$  is compiled once from measured device responses and predicts capability for any payload, and the two-channel decomposition lets each failure mode be diagnosed and remedied independently. Timing-based address selection in spiking networks [19] and driven-dissipative mode competition [10, 13] provide candidate physical selectors.

*Evidence hierarchy*. Four layers, in decreasing rigor: (i) exact theorem (full-rank dictionary gives universal payload realizability); (ii) approximate theory (conditioning, drift, and stereotypy bounds); (iii) phenomenol-

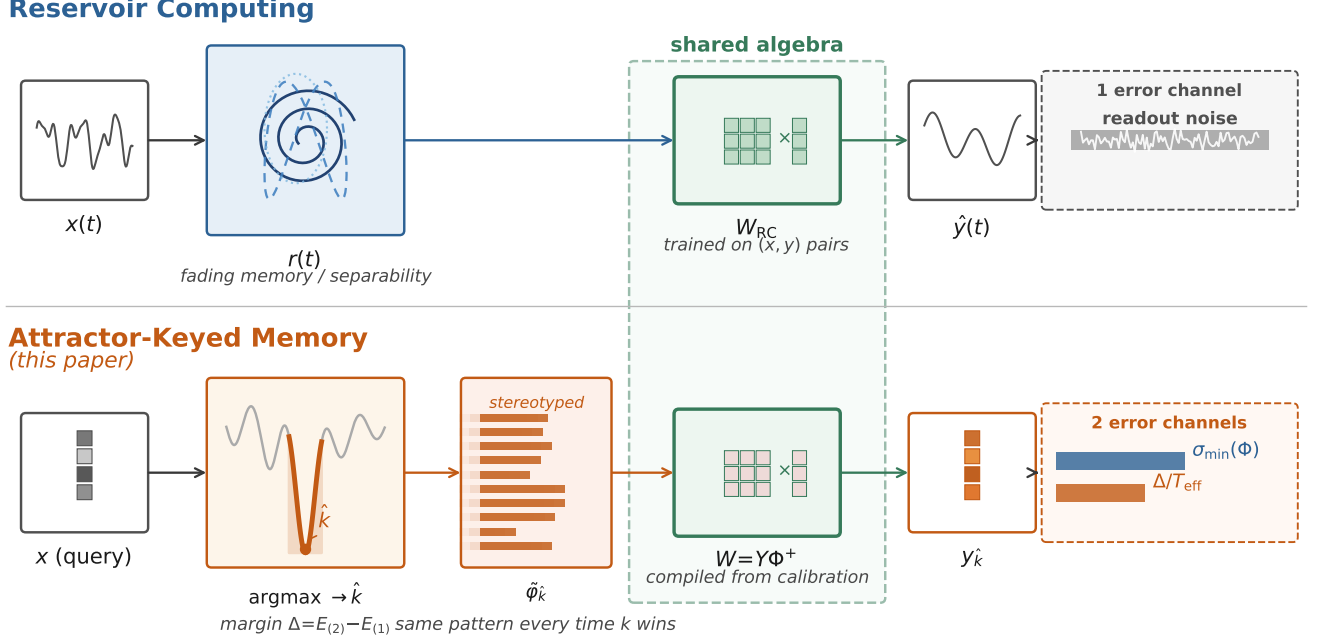


FIG. 1. **Attractor-keyed memory versus reservoir computing.** Both use a linear readout from a physical state, but differ structurally: reservoirs operate on a *continuous* driven trajectory, AKM on a *discrete* set of attractor signatures; reservoir states are *input-sensitive* (separability), AKM signatures are *stereotyped* (same pattern each time route  $k$  wins); the reservoir decoder is *trained* on input–output pairs, the AKM decoder is *compiled* from calibration data via  $W = Y\Phi^+$ ; reservoir analyses fold routing-like failures into an overall readout error budget, AKM decomposes into *two* separately diagnosable channels (decoding fidelity  $\sigma_{\min}(\Phi)$ , routing reliability  $\Delta/T_{\text{eff}}$ ); reservoir analysis yields a capacity bound, AKM yields a predeployment *certification protocol*. In AKM the payload  $y_k$  need not resemble the attractor state; the attractor is the key, not the stored value.

ogy (Gibbs routing fit); (iv) synthetic validation (Monte Carlo on speckle-signature models, not physical experiment). The synthetic validation confirms internal consistency of the analytic predictions; it does not test stereotypy or any other physical assumption. Figure 1 contrasts the architecture with reservoir computing; Fig. 2(a) illustrates a photonic realization. Whether real competitive selectors satisfy stereotypy is the central open experimental question; the formal statement and its quantitative relaxation appear below. Compatibility with gradient-based training is demonstrated in the Supp. Mat. [20].

*Route–decode abstraction.* Fetchless lookup factors into routing and readout:

$$x \mapsto \hat{k}(x) \mapsto \tilde{\phi}_{\hat{k}(x)} \mapsto y = W\tilde{\phi}_{\hat{k}(x)}. \quad (1)$$

Here  $x \in \mathbb{R}^N$  is an  $N$ -dimensional input;  $\hat{k}(x)$  is the discrete route selected by the physical competition;  $\tilde{\phi}_{\hat{k}(x)} \in \mathbb{R}^{M_{\text{sig}}}$  is the single-shot measured signature of the winning state; and  $W \in \mathbb{R}^{D \times M_{\text{sig}}}$  is a fixed linear decoder mapping signatures to  $D$ -dimensional payloads. The theory requires only that routing returns a winner  $\hat{k}(x)$  with a measurable margin, and that decoding acts on the win-

ner’s signature; the internal structure of the selector is an implementation detail.

*Score generation and routing.* One realization maps an input  $x$  to a bank of  $M_{\text{score}} \geq K$  candidate scores:

$$h(x) = B_{\text{wide}} x, \quad B_{\text{wide}} \in \mathbb{R}^{M_{\text{score}} \times N}. \quad (2)$$

In photonic platforms  $B_{\text{wide}}$  may be realized by a programmable linear optical transformation [21–23]. A fixed routing map  $R_{\text{route}} \in \mathbb{R}^{K \times M_{\text{score}}}$  compresses the wide scores into  $K$  competing routes:

$$g(x) = R_{\text{route}} h(x) \in \mathbb{R}^K, \quad E_k(x) = -g_k(x), \quad (3)$$

where  $g_k(x)$  is the score for route  $k$  and  $E_k(x)$  the corresponding selector energy. The selector returns  $\hat{k}(x) \in \arg \max_k g_k(x)$  with winner-to-runner-up margin

$$\Delta(x) = g_{(1)}(x) - g_{(2)}(x), \quad (4)$$

where  $g_{(1)} \geq g_{(2)} \geq \dots$  are the ordered scores. Since  $E_k = -g_k$ , this score-space margin equals the energy-space gap  $E_{(2)} - E_{(1)}$ ; we use  $\Delta$  for both throughout. Equations (2)–(4) describe one realization; the remainder of the theory depends only on the existence of a win-

ner  $\hat{k}(x)$  and a margin  $\Delta(x)$ . We assume only that misrouting decreases monotonically with  $\Delta(x)$ , a property testable by repeated hardware trials.

*Signature emission and decoding.* After routing converges to state  $u^{(k)}$ , a fixed measurement map  $\mathcal{M}$  produces the signature

$$\tilde{\phi}_k = \mathcal{M} u^{(k)} + \delta \in \mathbb{R}^{M_{\text{sig}}}, \quad (5)$$

where  $\delta$  is zero-mean measurement noise (decomposed in Supp. Mat., Sec. S3D into an input-dependent residual  $\varepsilon_k(x)$  and a stochastic component  $\delta_k$ ). Conditioned on selecting route  $k$ , the measured signature has mean  $\bar{\phi}_k$  and covariance  $\Sigma_k$ .

*Assumption (route-conditioned repeatability / stereotypy).* Conditioned on route  $k$  winning, shot-to-shot variation in  $\tilde{\phi}_k$  is dominated by device noise, not by differences in the triggering input  $x$ . This holds when competition is strong enough that each attractor basin funnels all initial conditions toward a single final state. When competition is weak and the winning state retains memory of the input,  $\Phi$  becomes a poor summary. Mode hopping or near-degeneracy can break stereotypy and must be diagnosed (Supp. Mat., Sec. S3).

Calibration forces each route in turn, records repeated trials, and collects the mean signatures and desired payloads:

$$\Phi = [\bar{\phi}_1 \cdots \bar{\phi}_K] \in \mathbb{R}^{M_{\text{sig}} \times K}, \quad Y = [y_1 \cdots y_K] \in \mathbb{R}^{D \times K}.$$

The dictionary  $\Phi$  is empirical, compiled from measured device responses. Runtime readout uses a fixed linear decoder  $y = W \tilde{\phi}_{\hat{k}(x)}$ , with  $W \in \mathbb{R}^{D \times M_{\text{sig}}}$ .

*Block-parallel architecture.*  $B$  independent blocks operate in parallel, each running its own physical  $\arg \max$  over  $K$  routes; the rank condition applies per block. The layer output is the sum of decoded signatures across all  $B$  blocks (Supp. Mat. [20]). Figure 2(a) illustrates the pipeline.

*Proposition 1 (Universal payload realizability).* The system  $W\Phi = Y$  admits a solution for every  $Y \in \mathbb{R}^{D \times K}$  if and only if  $\text{rank}(\Phi) = K$ . When this holds,  $M_{\text{sig}} \geq K$  and the minimum-norm exact decoder is  $W_\star = Y\Phi^+$  (proof and full decoder family in Supp. Mat. [20]). The condition is well known; what matters here is its *physical interpretation*: the  $K$  routes must produce  $K$  linearly independent measured patterns, and a single SVD of  $\Phi$  checks this before any task is specified.

If  $\text{rank}(\Phi) = r < K$ , exact decoding may still hold for a particular  $Y$  whose rows lie in  $\text{Row}(\Phi)$ . Rank deficiency rules out *universal* fetchless lookup, not every structured task. The challenge is not merely to produce a stable winner; it is to produce  $K$  selected states whose measured signatures span a  $K$ -dimensional space.

*Selector realizations.* The decoder theory is selector-agnostic, but two Ising constructions show the framework generates concrete hardware designs.

*One-hot QUBO (quadratic unconstrained binary optimization) selector.* Binary variables  $z_i \in \{0, 1\}$  define the energy

$$E_{\text{WTA}}(z; x) = \lambda \left( \sum_{i=1}^K z_i - 1 \right)^2 - \sum_{i=1}^K g_i(x) z_i, \quad \lambda > 0, \quad (6)$$

where  $\lambda$  is a penalty weight enforcing the one-hot constraint. If  $\lambda$  exceeds the largest score magnitude, every global minimizer is one-hot and satisfies  $i^\star \in \arg \max_i g_i(x)$ : on the one-hot manifold,  $E_{\text{WTA}}(e_i; x) = -g_i(x)$ , recovering the selector energy of Eq. (3). The standard spin transformation  $z_i = (1 + s_i)/2$  yields an equivalent Ising Hamiltonian with dense antiferromagnetic couplings and local fields proportional to  $g_i(x)$ . Each block in the parallel architecture realizes its own such QUBO. The full proof is given in the Supp. Mat. [20].

*Binary comparator ( $K = 2$ ).* An antiferromagnetically coupled spin pair with coupling  $J > 0$  and local fields  $h_a(x), h_b(x)$  acts as a single-bit selector returning  $\text{sign}(h_a - h_b)$ , the physical analogue of the compare-and-concatenate operation [3]. When the coupling exceeds the field magnitudes, every ground state is anti-aligned and the energy gap is  $\Delta_{\text{cmp}}(x) = 2|h_a(x) - h_b(x)|$ . Chaining  $n_c$  such comparators produces an  $n_c$ -bit address into a  $2^{n_c}$ -entry lookup table. Sweeping the field difference and comparing the empirical misrouting rate against  $\Delta_{\text{cmp}}/T_{\text{eff}}$  is the simplest experimental test of fetchless lookup.

Driven-dissipative oscillators offer a third realization (Supp. Mat. [20]).

*Robustness: two separable failure channels.* At run time, two kinds of errors remain: perturbations of the signature after the correct route wins, and selection of the wrong route. We decompose expected error by conditioning on the routing outcome. In physical devices the same noise sources may influence both mechanisms, so the decomposition is a diagnostic tool, not a claim of statistical independence (see Supp. Mat. [20], Remark 3).

*Conditional decoding error.* If route  $k$  wins and the single-shot signature is  $\tilde{\phi}_k = \bar{\phi}_k + \delta$  (with perturbation  $\delta$  aggregating shot noise, detector noise, and drift), the minimum-norm decoder gives (using  $W\bar{\phi}_k = y_k$ )

$$\|W\tilde{\phi}_k - y_k\|_2 = \|Y\Phi^+\delta\|_2 \leq \frac{\|Y\|_2}{\sigma_{\min}(\Phi)} \|\delta\|_2, \quad (7)$$

where  $\|Y\|_2$  is the spectral norm of the payload table. For zero-mean fluctuations with covariance  $\Sigma_k$ ,

$$\mathbb{E}\|W\tilde{\phi}_k - y_k\|_2^2 = \text{Tr}[Y\Phi^+\Sigma_k(\Phi^+)^T Y^T] \leq \frac{\|Y\|_2^2}{\sigma_{\min}(\Phi)^2} \text{Tr}\Sigma_k. \quad (8)$$

Tikhonov regularization can trade exactness for improved noise robustness; see Supp. Mat. [20]. When stereotypy

is imperfect and the residual input-dependent shift has norm at most  $\varepsilon_{\text{stereo}}$ , the additional decoding error is bounded by  $\|Y\|_2 \varepsilon_{\text{stereo}}/\sigma_{\min}(\Phi)$  (Supp. Mat. [20]), so stereotypy need only hold to within the device noise floor.

*Dictionary drift.* If the dictionary drifts from  $\Phi_0$  at calibration to  $\Phi_0 + \delta\Phi(t)$  while the decoder remains  $W_0 = Y\Phi_0^+$ ,

$$\|W_0[\Phi_0 + \delta\Phi(t)] - Y\|_2 \leq \frac{\|Y\|_2}{\sigma_{\min}(\Phi_0)} \|\delta\Phi(t)\|_2. \quad (9)$$

Recalibration is needed once the drift exceeds a user-specified tolerance  $\varepsilon_{\text{tol}} \sigma_{\min}(\Phi_0)$ ; see Supp. Mat. [20] for the explicit criterion.

*Routing error.* If the intended route is  $k^*$  but the selector returns  $\ell \neq k^*$ , no decoder can repair the mistake. We use the Gibbs form only as a phenomenological fit to routing statistics, not as a microscopic claim; the theory needs one empirical property: larger margin means lower misrouting. Modeling route probabilities as

$$P(k) = \frac{e^{-E_k/T_{\text{eff}}}}{\sum_j e^{-E_j/T_{\text{eff}}}}, \quad (10)$$

where  $E_k(x) = -g_k(x)$  is the selector energy defined in Eq. (3) and  $T_{\text{eff}}$  is an effective temperature fitted from repeated trials [11, 13, 24], the misrouting probability satisfies

$$P_{\text{mis}} \leq \frac{(K-1)e^{-\Delta/T_{\text{eff}}}}{1 + (K-1)e^{-\Delta/T_{\text{eff}}}}, \quad (11)$$

where  $\Delta = \min_{k \neq k^*} (E_k - E_{k^*})$  is the minimum energy gap to the next competing route (equal to the score-space margin of Eq. (4), since  $E_k = -g_k$ ). The bound follows because each competitor contributes at most  $e^{-\Delta/T_{\text{eff}}}$  to the partition function, and  $P_{\text{mis}} = S/(1+S)$  is monotone in  $S = \sum_{k \neq k^*} e^{-(E_k - E_{k^*})/T_{\text{eff}}}$ . For  $\Delta \gg T_{\text{eff}}$ , the log-odds of correct routing scale linearly in  $\Delta/T_{\text{eff}}$ , which is directly testable. If  $d_Y = \max_{k,\ell} \|y_k - y_\ell\|_2$  is the payload diameter, a misrouted trial incurs both a payload mismatch and decode noise on the wrong route; a first-moment bound via the triangle inequality gives a routing contribution at most  $P_{\text{mis}}(d_Y + \|Y\|_2 \bar{\delta}/\sigma_{\min}(\Phi))$ , where  $\bar{\delta} = \max_k \sqrt{\text{Tr} \Sigma_k}$  is the worst-case per-route noise level. A tighter second-moment decomposition is given in the Supp. Mat. (Remark 3), where the solid analytic curves in Fig. 2(c–f) are derived; it requires the additional modeling assumption that route-conditioned emission noise has zero mean and covariance  $\Sigma_\ell$  on each route  $\ell$ , independently of which route was intended (see Supp. Mat. for the precise statement and caveats). Whether the Gibbs fit is adequate must be assessed by goodness-of-fit testing on binned route frequencies; we report fit quality rather than assume it.

Figure 2(b–f) illustrates the decomposition on a controlled speckle-signature model (Monte Carlo simulation;

see Supp. Mat., Fig. S1 for individual diagnostic plots of each failure mode). Because the simulation draws routes from the same Gibbs model used to derive Eq. (11), the agreement in Fig. 2(c,f) confirms the algebra, not the physical adequacy of the Gibbs assumption; that requires a goodness-of-fit test on real route frequencies, not yet available.

*Calibration and training.* Fetchless lookup operates on two time scales. A slow calibration stage forces each route, measures signature statistics, forms  $\Phi$ , and compiles  $W = Y\Phi^+$ . Between recalibrations,  $\Phi$  is fixed and online learning updates only the payload matrix  $Y$ , touching one column per sample (winner-sparse updates). This alters  $W$  by a rank-1 update determined by  $\Phi^+$ ; backpropagation through the nondifferentiable  $\arg \max$  uses a top-two surrogate gradient. Full derivation, gradient-starvation mitigations, and a training experiment are in the Supp. Mat. [20].

*Experimental protocol and falsifiability.* Four steps translate the theory into a falsifiable experiment: **(1)** Force each route in turn and record  $R$  repeated signature measurements. This determines the sample-mean dictionary  $\hat{\Phi}$  (the finite-sample estimate of  $\Phi$ ), the covariances  $\Sigma_k$ , the empirical rank,  $\sigma_{\min}(\hat{\Phi})$ , and the stereotypy diagnostic  $\varepsilon_{\text{stereo}}/\sqrt{\text{Tr} \Sigma_k}$  (Supp. Mat., Sec. S3). Full rank is confirmed only if a bootstrap confidence interval for  $\sigma_{\min}(\hat{\Phi})$ , constructed by resampling the  $R$  calibration trials, excludes zero; the interval's lower endpoint provides a conservative bound on dictionary conditioning. Under the hypothesis that centered signatures are sub-Gaussian with  $\sigma_{\text{sg},k}^2 \leq \|\Sigma_k\|_2$  (satisfied by Gaussian noise; see Supp. Mat., Proposition 2 for the precise statement), the number of trials needed to resolve  $\sigma_{\min}(\Phi)$  scales as  $R = O(K \|\Sigma\|_2 (M_{\text{sig}} + \log K)/\sigma_{\min}(\Phi)^2)$  (Supp. Mat., Proposition 2). If  $\text{rank}(\Phi) < K$ , no linear decoder can realize universal fetchless lookup. **(2)** Compile  $W = Y\Phi^+$  for test payloads and verify  $W\Phi \approx Y$  on forced-route means; compare single-shot error scaling with  $\sigma_{\min}(\Phi)$  via Eqs. (7)–(8). **(3)** Release the selector, record winner frequencies versus the measured top-two margin, and fit  $T_{\text{eff}}$ . Assess the Gibbs fit by a goodness-of-fit test (e.g.,  $\chi^2$  on binned route frequencies); test Eq. (11). A necessary consistency check: compare the signatures emitted under free-running competition with the forced-route means in  $\hat{\Phi}$ . If forcing bypasses competition dynamics, it may induce a systematic bias that the calibrated dictionary does not capture. A statistically significant shift between forced and free signatures indicates that the calibration model requires correction or that a free-running calibration protocol is needed. **(4)** Monitor drift in mean signatures over time. Recalibrate when  $\|\delta\Phi(t)\|_2$  exceeds  $\varepsilon_{\text{tol}} \sigma_{\min}(\Phi_0)$ , the tolerance derived from Eq. (9).

No hardware demonstration exists to date; the protocol defines the criteria a first experiment must satisfy. The required ingredients (high-dimensional signa-

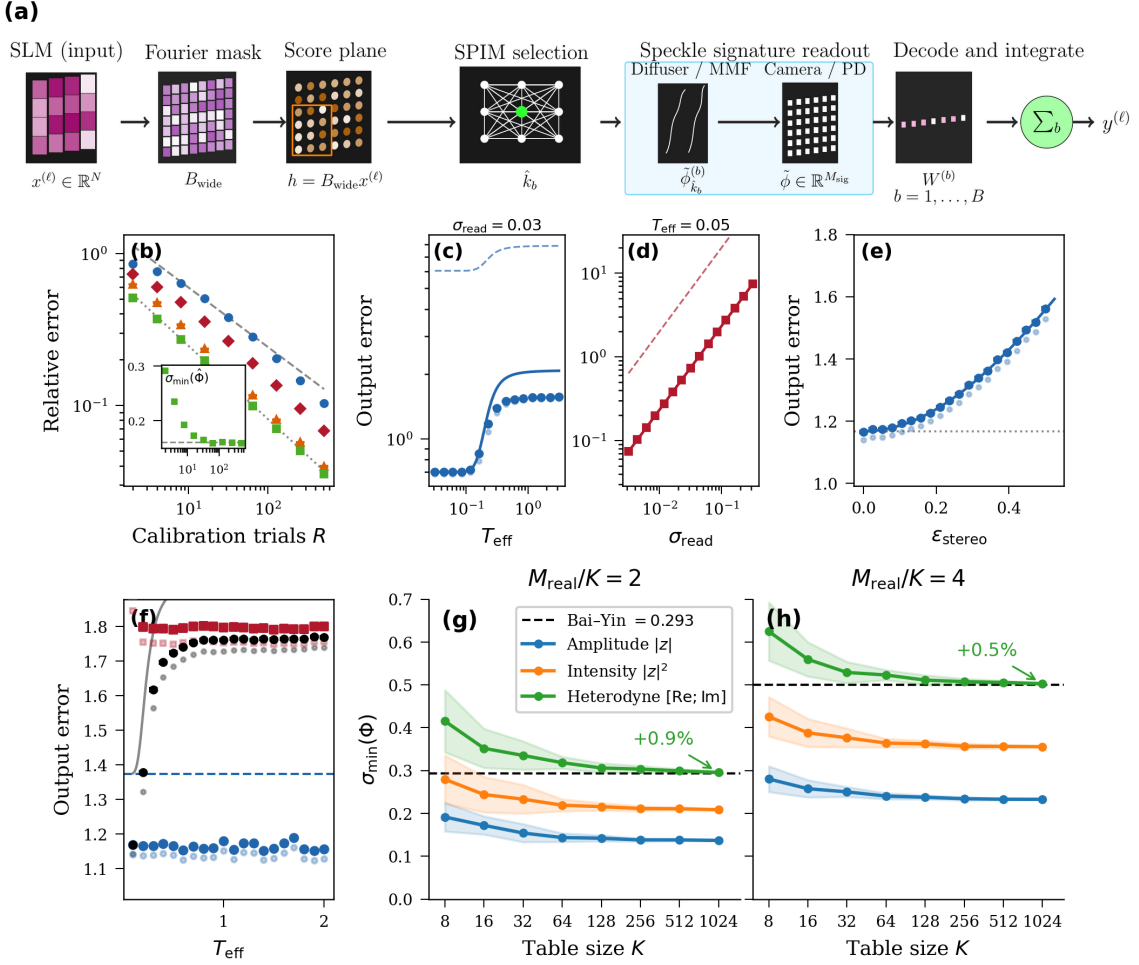


**FIG. 2. Photonic implementation and numerical validation of attractor-keyed memory.** (a) Schematic photonic pipeline. A spatial light modulator (SLM) encodes the input  $x$ ; a Fourier mask implements  $B_{\text{wide}}$ , producing candidate scores. A block-diagonal routing map  $R_{\text{route}}$  compresses scores into  $K$  competing routes. A spatial photonic Ising machine (SPIM) [25] selects the winner  $\hat{k}_b$  with margin  $\Delta$ . The selected mode's field propagates through a scattering medium (diffuser or multimode fiber); a detector array records the speckle signature  $\tilde{\phi}_{\hat{k}_b} \in \mathbb{R}^{M_{\text{sig}}}$ . A pre-compiled decoder  $W^{(b)}$  maps each signature to output; summing over  $B$  blocks yields  $y$ . (b)–(f) Error decomposition on a controlled speckle-signature model (Monte Carlo, not experiment;  $K = 64$ ,  $M_{\text{sig}} = 128$ ,  $D = 16$ ;  $R$ : calibration trials per route;  $\sigma_{\text{read}}$ : readout noise s.d.). (b) Relative reconstruction error  $\|W_{\hat{\Phi}} \Phi - Y\|_F / \|Y\|_F$  versus calibration trials  $R$ , where  $W_{\hat{\Phi}} = Y \hat{\Phi}^+$  is the decoder compiled from the noisy estimate  $\hat{\Phi}$  and  $\Phi$  is the true mean-signature dictionary; four dictionary types (amplitude  $|z|$ , intensity  $|z|^2$ , heterodyne  $[\Re z; \Im z]$ , orthogonal);  $\sigma_{\min}(\Phi)$  controls convergence rate. (c)–(f) All four panels use the amplitude-speckle dictionary. Solid lines: analytic RMS prediction  $\sqrt{\mathbb{E}\|e\|_2^2}$  from the two-channel second-moment decomposition (Supp. Mat., Remark 3, Eq. (S17); see text for modeling assumptions); filled circles: Monte Carlo RMS (10,000 trials); faint circles: Monte Carlo mean  $\mathbb{E}\|e\|_2$ , which lies  $\approx 2.5\%$  below the RMS by Jensen's inequality (Supp. Mat., Remark 1); dashed: expected worst-case bounds obtained by multiplying per-trial bounds (Eq. (7) for decoding;  $d_Y + \|Y\|_2 \bar{\delta} / \sigma_{\min}(\Phi)$  for a single misrouted trial) by appropriate probabilities, with  $P_{\text{mis}}$  from Eq. (11). (c) Routing-dominated regime (varying  $T_{\text{eff}}$  at fixed  $\sigma_{\text{read}} = 0.03$ ). (d) Decoding-dominated regime (varying  $\sigma_{\text{read}}$  at fixed  $T_{\text{eff}} = 0.05$ ). The two error channels are separable and each matches its predicted scaling. (e) Decoding error under stereotypy violation  $\varepsilon_{\text{stereo}}$  (correct routing enforced). (f) Full pipeline at a realistic operating point; the crossover at  $T_{\text{eff}} \approx 0.71$  separates the decoding-limited from the routing-limited regime. (g), (h) Dictionary conditioning  $\sigma_{\min}(\Phi)$  versus table size  $K$  at fixed real aspect ratio  $M_{\text{real}}/K$ , where  $M_{\text{real}}$  is the real signature dimensionality ( $M_{\text{sig}}$  for real-valued modalities,  $2M_c$  for heterodyne with  $M_c$  complex modes). Three measurement modalities, 30 random seeds per point; shaded bands:  $\pm 1$  s.d. (g)  $M_{\text{real}}/K = 2$ . (h)  $M_{\text{real}}/K = 4$ . From  $K = 64$  onward,  $\sigma_{\min}$  tracks the Bai-Yin prediction (dashed) with modest finite-size corrections at small  $K$ . At  $K = 1024$  the heterodyne value lies within 1% of the asymptote at both aspect ratios. See Supp. Mat. [20] for full panel specifications.

tures in photonic reservoirs [17, 26], stable linear readout in programmable interferometric systems [21–23, 27],

and competitive mode selection in driven-dissipative oscillators [11, 13, 28]) exist separately in current plat-

forms; integrating them into a single device remains open. A forced-routing dictionary measurement is the natural first experiment, followed by a  $K = 2$  routing test of the predicted  $\Delta_{\text{cmp}}/T_{\text{eff}}$  dependence.

*Scope and outlook.* How far the scheme scales depends on the oversampling ratio  $M_{\text{sig}}/K$ . The Bai–Yin law predicts that  $\sigma_{\text{min}}(\Phi)$  stays bounded away from zero when  $M_{\text{sig}}/K$  exceeds unity by a finite factor; at  $M_{\text{sig}}/K = 2$  this already yields low error amplification in Eqs. (7)–(8). Orthogonal constructions achieve optimal conditioning (condition number one) by design. Real device signatures may exhibit spatial correlations that reduce the effective degrees of freedom below  $M_{\text{sig}}$ , worsening conditioning relative to the Bai–Yin prediction; the SVD diagnostic detects this. At  $K = 1024$  with  $M_{\text{real}}/K = 2$ , heterodyne conditioning lies within 1% of the Bai–Yin asymptote and is flat from  $K = 64$  onward [Fig. 2(g, h)], extending the framework to table sizes relevant to mixture-of-experts routing ( $K \sim 10^2$ – $10^3$ ). Among the three modalities tested [Fig. 2(b) and (g, h)], phase-sensitive (heterodyne) readout achieves the best conditioning, improving  $\sigma_{\text{min}}$  by  $3.4\times$  over amplitude-only measurement at matched complex-mode count; the gain decomposes roughly 2:1 between intrinsic phase sensitivity and doubled real channel count (Supp. Mat., Fig. S2).

AKM replaces an  $O(D)$  memory read with an  $M_{\text{sig}}$ -channel measurement followed by a  $D \times M_{\text{sig}}$  linear decode. This trade is favorable when the decode is performed natively in the measurement hardware (e.g., an optical linear projection) or when data-movement cost dominates compute [2, 7]; it is unfavorable if the decode requires a separate digital matrix-vector multiply at large  $M_{\text{sig}}$ . At  $M_{\text{sig}}/K = 2$  with digital decode, break-even requires either native optical decode or DRAM-resident payloads (Supp. Mat., Sec. S13). The primitive does not replace memory in general; it targets architectures where the decode can be absorbed into the measurement optics, or where payload storage lives off-chip [7].

Any competitive physical selector that produces high-dimensional signatures and settles to stereotyped attractor states is a candidate platform: coherent Ising machines, polariton condensate networks, laser arrays, and spatial photonic Ising machines (SPIMs) all produce post-selection fields far richer than a single index. Among these, the SPIM platform [the photonic selector shown in Fig. 2(a)] is closest to the requirements, owing to two recent advances. First, focal-plane division has made SPIMs fully programmable for arbitrary Ising problems, including the one-hot QUBO selector of Eq. (6), with experimentally demonstrated ground-state solutions for up to 32-spin max-cut instances and favorable simulated scaling beyond [29]. Second, full-aperture wavefront retrieval and correction has removed the optical-aberration bottleneck that previously confined operation to a restricted SLM region [30], increasing the effective  $M_{\text{sig}}$  per route and with it the oversampling ratio on which

dictionary conditioning depends. Programmable competitive selection and high-dimensional optical readout are thus individually operational on a single hardware family. What remains untested is the quantity AKM requires: within-attractor variance of the full speckle signature, conditioned on the same winning route.

Two open experimental questions set the practical ceiling: *whether* real device signatures satisfy stereotypy, and *how fast* the dictionary drifts. Indirect evidence is encouraging but does not directly test the required metric. Speckle-based PUFs achieve  $\sim 94\%$  bit-level reproducibility across thousands of response dimensions [31, 32]. Photonic reservoir computers exhibit near-unity ( $> 0.95$ ) state-consistency correlations in injection-locked regimes [17, 33]. Trapped polariton condensates maintain spin-bifurcated attractor states with  $\sim 95\%$  circular-polarisation purity and dwell times exceeding seconds [34, 35]. Coherent Ising machines have unique mean-field steady-state amplitudes for each spin configuration [24], though amplitude reproducibility under noise remains experimentally uncharacterised. In every case, reproducibility of the *discrete outcome* (which attractor is selected) is what gets measured; reproducibility of the *continuous high-dimensional physical state* within a given attractor is almost never quantified (Supp. Mat. [20]).

The specific measurement AKM requires has not been reported for any competitive selector, but the data likely already exist. What is needed: record the full continuous-valued output (CIM pulse amplitudes, SPIM pixel intensities, or polariton emission profiles) across many trials, condition on reaching the same discrete attractor, and compute the within-basin pattern covariance. From this one obtains  $\Phi$ ,  $\sigma_{\text{min}}(\Phi)$ ,  $\Sigma_k$ , and  $\varepsilon_{\text{stereo}}$ , the four quantities that determine whether a given platform can support fetchless lookup at a target scale. The forced-routing protocol described above provides the concrete path.

The author acknowledges support from HORIZON EIC-2022-PATHFINDERCHALLENGES-01 HEISINGBERG Project 101114978, from Weizmann–UK Make Connection Grant 142568, and from the EPSRC UK Multidisciplinary Centre for Neuromorphic Computing (grant UKRI982).

---

\* N.G.Berloff@damtp.cam.ac.uk

- [1] W. Fedus, B. Zoph, and N. Shazeer, Switch transformers: Scaling to trillion parameter models with simple and efficient sparsity, arXiv:2101.03961 [cs.LG].
- [2] V. Sze, Y.-H. Chen, T.-J. Yang, and J. S. Emer, Proceedings of the IEEE **105**, 2295 (2017).
- [3] E. Izhikevich, Spiking manifesto (2025), arXiv:2512.11843 [cs.NE].
- [4] Y. Shen, N. C. Harris, S. Skirlo, M. M. Prabhu, T. Baehr-Jones, M. Hochberg, X. Sun, S. Zhao, H. Larochelle, D. Englund, and M. Soljačić, Nature Photonics **11**, 441

- (2017).
- [5] A. N. Tait, T. F. De Lima, E. Zhou, A. X. Wu, M. A. Nahmias, B. J. Shastri, and P. R. Prucnal, *Scientific Reports* **7**, 7430 (2017).
- [6] W. A. Wulf and S. A. McKee, *ACM SIGARCH computer architecture news* **23**, 20 (1995).
- [7] M. Horowitz, in *2014 IEEE international solid-state circuits conference digest of technical papers (ISSCC)* (IEEE, 2014) pp. 10–14.
- [8] J. L. Hennessy and D. A. Patterson, *Communications of the ACM* **62**, 48 (2019).
- [9] S. Williams, A. Waterman, and D. A. Patterson, *Communications of the ACM* **52**, 65 (2009).
- [10] N. G. Berloff *et al.*, *Nature Materials* **16**, 1120 (2017).
- [11] P. L. McMahon, A. Marandi, Y. Haribara, R. Hamerly, C. Langrock, S. Tamate, T. Inagaki, H. Takesue, S. Utsunomiya, K. Aihara, R. L. Byer, M. M. Fejer, H. Mabuchi, and Y. Yamamoto, *Science* **354**, 614 (2016).
- [12] T. Honjo *et al.*, *Science Advances* **7**, eabh0952 (2021).
- [13] N. Stroeve and N. G. Berloff, *Advanced Quantum Technologies* **6**, 2300055 (2023).
- [14] R. Penrose, *Mathematical Proceedings of the Cambridge Philosophical Society* **51**, 406 (1955).
- [15] H. Jaeger and H. Haas, *Science* **304**, 78 (2004).
- [16] J. Dambre, D. Verstraeten, B. Schrauwen, and S. Massar, *Scientific Reports* **2**, 514 (2012).
- [17] D. Brunner, M. C. Soriano, C. R. Mirasso, and I. Fischer, *Nature Communications* **4**, 1364 (2013).
- [18] H. Ramsauer, B. Schäfl, J. Lehner, P. Seidl, M. Widrich, T. Adler, L. Gruber, M. Holzleitner, M. Pavlović, G. K. Sandve, *et al.*, arXiv preprint arXiv:2008.02217 (2020).
- [19] N. G. Berloff, Polychronous wave computing: Timing-native address selection in spiking networks (2026), arXiv:2601.13079 [cond-mat.dis-nn].
- [20] See supplemental material, at [[https://www.damtp.cam.ac.uk/user/ngb23/publications/SI\\_AKM.pdf](https://www.damtp.cam.ac.uk/user/ngb23/publications/SI_AKM.pdf)] for soft-spin dynamics, binary comparator details, ridge regularization, training derivations, experiment specification,  $\sigma_{\min}$  scaling analysis, and reproducible code.
- [21] D. A. B. Miller, *Photonics Research* **1**, 1 (2013).
- [22] W. R. Clements, P. C. Humphreys, B. J. Metcalf, W. S. Kolthammer, and I. A. Walmsley, *Optica* **3**, 1460 (2016).
- [23] T. Onodera, M. M. Stein, B. A. Ash, M. M. Sohoni, M. Bosch, R. Yanagimoto, M. Jankowski, T. P. McKenna, T. Wang, G. Shvets, M. R. Shcherbakov, L. G. Wright, and P. L. McMahon, *Nature Physics* 10.1038/s41567-025-03094-2 (2025).
- [24] R. Hamerly, L. Bernstein, A. Sludds, M. Soljačić, and D. Englund, *Physical Review X* **9**, 021032 (2019).
- [25] D. Pierangeli, G. Marcucci, and C. Conti, *Physical Review Letters* **122**, 213902 (2019).
- [26] T. W. Hughes, I. A. D. Williamson, M. Minkov, and S. Fan, *Science Advances* **5**, eaay6946 (2019).
- [27] S. Pai, Z. Sun, T. W. Hughes, T. Park, B. Bartlett, I. A. D. Williamson, M. Minkov, M. Milanizadeh, N. Abebe, F. Morichetti, A. Melloni, S. Fan, O. Solgaard, and D. A. B. Miller, *Science* **380**, 398 (2023).
- [28] K. P. Kalinin and N. G. Berloff, *Physical Review Letters* **121**, 235302 (2018).
- [29] D. Veraldi, D. Pierangeli, S. Gentilini, M. Calvanese Strinati, J. Sakellariou, J. S. Cummins, A. Kamaletdinov, M. Syed, R. Z. Wang, N. G. Berloff, D. Karanikolopoulos, P. G. Savvidis, and C. Conti, *Physical Review Letters* **134**, 063802 (2025).
- [30] D. Karanikolopoulos, P. Karavelas, L. Mouchliadis, A. Spiliotis, N. Pitanios, S. Gentilini, D. Veraldi, P. Charlesworth, D. Pierangeli, J. Sakellariou, *et al.*, arXiv preprint arXiv:2602.13714 (2026).
- [31] Y. Gao, S. F. Al-Sarawi, and D. Abbott, *Nature Electronics* **3**, 81 (2020).
- [32] R. Pappu, B. Recht, J. Taylor, and N. Gershenfeld, *Science* **297**, 2026 (2002).
- [33] N. Oliver, T. Jüngling, and I. Fischer, *Physical Review Letters* **114**, 123902 (2015).
- [34] H. Ohadi, A. Dreismann, Y. G. Rubo, F. Pinsker, Y. del Valle-Inclan Redondo, S. I. Tsintzos, Z. Hatzopoulos, P. G. Savvidis, and J. J. Baumberg, *Physical Review X* **5**, 031002 (2015).
- [35] Y. del Valle-Inclan Redondo, H. Ohadi, Y. G. Rubo, O. Beer, A. J. Ramsay, S. I. Tsintzos, Z. Hatzopoulos, P. G. Savvidis, and J. J. Baumberg, *New Journal of Physics* **20**, 075008 (2018).